AIAA 81-4245

Optimal Air-Breathing Launch Vehicle Design

Philip David Hattis*
The Charles Stark Draper Laboratory, Inc., Cambridge, Mass.

A generalized two-point boundary problem methodology, similar to techniques used in deterministic optimal control studies, is applied to the design and flight analysis of a two-stage air-breathing launch vehicle. Simultaneous consideration is given to configuration and trajectory by treating geometry, dynamic discontinuities, and time-dependent flight variables all as controls to be optimized with respect to a single mathematical performance measure. While minimizing fuel consumption, inequality constraints are applied to dynamic pressure and specific force. The optimal system fuel consumption and staging Mach number are found to vary little with changes in the inequality constraints due to substantial geometry and trajectory adjustments. Staging, from an air-breathing first stage to a rocket-powered second stage, consistently occurs near Mach 3.5. The dynamic pressure bound has its most pronounced effects on vehicle geometry, particularly the air-breathing propulsion inlet area, and on the first-stage altitude profile. The specific force has its greatest influence on the second-stage thrust history.

Nomenclature

A = adjoint coefficient matrix defined in Eq. (30)
B = simplifying matrix variable defined in Eq. (42b)
C_J = coefficient of cost contribution to control variations
C_Ψ = coefficient of constraint contribution to control variations
C = simplifying vector variable defined in Eq. (42b)
f = time derivative of state vector x
f_s^+, f_s^- = f evaluated at t_s^+, t_s^-
F = partial of f with respect to x
g = simplifying vector variable defined in Eq. (38)
G = partial of f with respect to u
h = scramjet inlet height
H = Hamiltonian function
I_{sp} = specific impulse
$I_{\Psi\Psi}, I_{\Psi J}, I_{JJ}$ = integral functions defined in Eqs. (42a)
J = mathematical cost function
K = partial of f with respect to p
L = mathematical cost contribution function requiring integration over time
m = mass
M = Mach number in aerodynamic equations; simplifying matrix variable defined in Eq. (38) used in variation equations
p = parameter vector
S = step size
t = time
u = control vector
U = positive definite, symmetric, time-dependent weighting matrix
v = simplifying vector variable defined in Eq. (38)
V = positive-definite symmetric weighting matrix
w = fuselage width
x = state vector
λ = costate vector
Λ = adjoint function defined in Eq. (29)
τ = takeoff time
ϕ = terminal time cost (fuel consumption)
Ψ = equality constraint vector
Ω = state integration cutoff function

Subscripts

f = fuel (propellant)
i = element of a set
s = scramjet (for physical variables); switch point (for time variables); and specified (for mathematical cost)
T = turbojet
f,p,u,x = variables with respect to which partial differentiation is done

Received July 3, 1980; revision received Nov. 17, 1980.

*Member of Technical Staff.

Introduction

At a time when the first reusable space transportation system is in the final development stages, considerable attention is being given to the design of vehicles with improved performance over what can be achieved with the Space Shuttle. Design improvements for advanced space transportation systems can be judged strictly on engineering performance. For example, the propellant mass consumption requirement for a variety of propulsion methods, and the sensitivity of this quantity to specific force and dynamic pressure constraints form an unambiguous performance measure with which to compare alternate space transportation concepts.

A launch vehicle that promises considerable reduction in propellant mass compared to Space Shuttle technology is the air-breathing launch system.

As generally proposed, the air-breathing launch vehicle is two-staged, with an air-breathing first stage and the second stage operating as a conventional rocket. In the present study, the first stage has turbojet engines operable to about Mach 3. At some point near Mach 1, dual-mode ramjet engines, with both subsonic and supersonic combustion capability, are phased into use, overlapping turbojet use. Between Mach 3 and Mach 12, separation of the stages occurs. The first stage returns as an aircraft, while the second attains orbital velocity.

At low Mach numbers, conventional jet fuel is assumed. For the ramjet and rocket phases, liquid hydrogen fuel is proposed.

A vehicle with these characteristics offers the advantages of full-system reusability, aircraft-type operation, safer abort procedures, and improved performance.

Many aspects of flight vehicle optimization have been addressed in the last 25 years, though generally individually. The Aerospace Research Laboratory developed an optimization technique to study the configuration of a two-dimensional hypersonic cruise vehicle using lift-to-drag ratio as the cost variable.[1] Optimal rocket trajectories with aerodynamic effects included have been calculated for fixed rocket configurations.[2] Minimum time-to-climb and maximum altitude paths have been computed for aircraft with specified geometry and performance models.[3] Attempts have recently been made to treat trajectory and configuration

simultaneously for a single-stage-to-orbit launch vehicle,[4] although the method iteratively optimizes each part separately.

When the aggregate objectives of these studies are considered, the need for a unified mathematical treatment to simultaneously optimize flight vehicle configuration and trajectory is clear.

This paper presents a methodology for optimization of the design of an air-breathing launch vehicle.[5] The procedure considers trajectory shape, aerodynamic design, propulsion system performance, and propulsion system changeover points. An efficient technique is devised for converging on a solution to the nonlinear two-point boundary value problem. The developed procedure is applied to a parametric analysis of the two-stage, air-breathing launch vehicle.

Problem Scope

Optimization of an air-breathing launch vehicle requires formulation of a mathematical model of the vehicle dynamics, the orbital mechanics, and the environment with a clear specification of the independent variables. The optimization criteria must also be established.

Independent Variable Relations

The vehicle considered is configured for horizontal takeoff. The payload to be delivered to low-Earth orbit is assumed comparable to the Space Shuttle. A parametric model of the vehicle includes aerodynamic geometry, propulsion geometry, fuel capacity, and propellant properties.

The basic first-stage dynamic behavior can be determined by giving consideration to wing, fuselage, and propulsion system dimensions, along with component mass models, propulsion system performance, and aerodynamic characteristics as a function of exterior geometry. For computational simplicity, only two-dimensional models are used. The fuselage geometry is characterized by flat angled upper and lower surfaces. The aft surface angle is assumed to be fixed at 12 deg, and its aerodynamic properties are incorporated into the installed propulsion system performance data. The vehicle nose angle, the fuselage width, and the overall length are left as parameters to be evaluated.

The fuselage mass is a function of surface area, propellant tank volume, and fuel type within a given tank. The fuselage surface contribution can be roughly estimated as 0.25 slugs/ft^2 (Ref. 6). The propellant tank contribution must be based on the volume available to each tank with the assumption that 80% of the total fuselage volume is available for fluid storage. The turbojet tank is constructed to contain a hydrocarbon fuel, while a cryogenic hydrogen tank is assumed for the scramjet. A parameter is created to specify the relative space allocation between the first-stage fuels.

The information necessary to characterize the propulsion system includes external geometry, mass, and operational performance. The geometry is defined by inlet height, with the entire fuselage width assumed utilized. The turbojet mass, extrapolated from advanced lightweight designs and historical weight reduction trends, is estimated at 5 slugs/ft^2 inlet area. The scramjet mass must be extrapolated from data on experimental configurations[7] designed to tolerate heat flux loads until well above Mach 6. The result is

$$m_s = (15.2h - 4.6/h)\,w \tag{1}$$

where m_s is in slugs if h and w are in feet.

Analysis of support system mass requirements suggest the bound[7]

$$m_s \geq 15.0\,w \qquad (m_s \text{ in slugs}) \tag{2}$$

With engine cowl loss effects incorporated, approximate propulsion performance data (see Ref. 8, p. 5) curve fits give

$$I_{sp_T} = 3800 - (300\,M) - (100\,M^2) \tag{3}$$

$$I \quad = 15\,000\,(M^{1.6})e^{-1.73(M^{0.52})} \tag{4}$$

It is assumed that if the scramjet and turbojet operate together then they are equally throttled. The mass capture ratio for the scramjet is required to model the spillage effects at low supersonic Mach numbers typical of these engines (see Ref. 8, p. 2).

A body-integrated delta wing is used and is treated as the sole source of aerodynamic lift and drag with coefficients available as a function of Mach number, aspect ratio, and angle of attack,[9] with a scaling factor used to approximate wing refinement and more complex geometries (~ 0.7 for drag, ~ 1.7 for lift). Parasitic drag is based on Shuttle zero angle of attack drag properties with a scale factor of 1/3 due to the very high drag from the Shuttle silica thermal protection tile surface.

The second stage is a scaled version of the Space Shuttle, somewhat refined to improve aerodynamics. The thrust is assumed selectable up to a parameterized maximum value. The propellant, a Shuttle-derived liquid hydrogen/liquid oxygen system, is internally carried. The planform area is derived by elementary scaling theory from volume. An 80% use of available volume for propellant storage is assumed. Mass is based on a scaling of Shuttle Orbiter 102 with a 15% reduction included to anticipate technology improvement. The second-stage aerodynamics are of the same nature as the Shuttle, but with the first-stage scaling factors to model refinements. The specific impulse of the rocket is held at 450 s. The independent geometric parameters are treated as elements of a parameter vector p, the elements of which are listed in the left column of Table 2.

The propulsion dynamics lead to three thrust magnitude discontinuities at switch times t_{s_i}, associated with propulsive mode changes. The first, following takeoff, represents transition from the turbojet-only mode to mixed turbojet/scramjet operation, the second represents transition to the scramjet-only mode, and the third represents simultaneous staging and initiation of the second-stage rocket thrust.

Two-dimensional orbital dynamics are used with an equatorial launch to equatorial orbit considered. The resulting state vector x has seven elements: angular and radial position, angular and radial velocity, and a mass state for each propulsive mode propellant quantity.

The atmosphere is assumed to be a perfect gas, its density is a function of altitude only, and the U.S. standard 1962/1976 atmosphere data is assumed.

Gravity is assumed to depend on altitude only, with variation modeled on a homogeneous sphere representation of the Earth.

Optimization Criteria

Optimization of the parameterized vehicle and its controls requires definition of the mathematical cost-function terms, choice of initial state boundary conditions, and specification of final state desired conditions.

Three quantities—fuel consumption, dynamic pressure, and specific force—are chosen to allow characterization of optimal performance. It is desired to minimize the total fuel consumption ϕ, where

$$\phi(x(\tau)) = m_{f_1}(\tau) + m_{f_2}(\tau) + m_{f_3}(\tau) \tag{5}$$

and where elements 1, 2, and 3 of m_f apply to the turbojet, scramjet, and rocket, respectively.

Dynamic pressure and specific force are bounded by use of a distributed penalty function L where

$$L(x(t),u(t),p) = L_1(x(t)) + L_2(x(t),u(t),p) \tag{6}$$

and where elements 1 and 2 of L apply to dynamic pressure and specific force, respectively. L_1 and L_2 are chosen so that 1) no penalty is assessed when the dynamic pressure and specific force remain within bounds; 2) penalties are assessed at increasing rates as the bound violations increase; and 3) no discontinuities in the penalty terms exist at the bounds.

The problem is treated backwards so that the initial state is the desired orbital state at burnout. A 75 mile circular orbit is appropriate, since it represents the fringe of the sensible atmosphere. The radial velocity vanishes and the angular velocity is independent of position. The angular position is arbitrarily set at zero as a convenient reference. The propellant vanishes as it should be exactly enough to achieve orbit.

At the terminal time, the takeoff conditions are needed. For horizontal takeoff altitude vanishes (sea level), radial velocity vanishes, angular velocity matches that of the desired takeoff speed of 250 mph, and angular position is a function of the initial reference value at orbit. The propellant masses should match the mass capacities of the propellant tanks, preventing excessive or insufficient vehicle dry mass in the solution.

Optimization Algorithm

Suppose system dynamics are expressed in equation form with state variable x. Define

$$\dot{x}=\frac{\mathrm{d}x}{\mathrm{d}t}=f(x,u,p,t_s) \tag{7}$$

Define the cost function $J(\tau)$ as

$$J(\tau)=\phi(x(\tau))+\int_{\tau}^{0}L(x(t),u(t),p(t))\,\mathrm{d}t \tag{8}$$

A Hamiltonian function, appropriate to finding an extremal of the cost, is

$$H=L+\lambda^T f \tag{9}$$

An optimal set of states, controls, parameters, and switch times are found by minimizing J. Differentiating Eq. (8) yields

$$\mathrm{d}J=\phi_x\mathrm{d}x(\tau+\mathrm{d}\tau)+\int_{\tau}^{0}(L_x\delta x+L_u\delta u+L_p\delta p)\,\mathrm{d}t-L\,|_{\tau}\mathrm{d}\tau \tag{10}$$

To first order,

$$\mathrm{d}x(\tau+\mathrm{d}\tau)=\delta x(\tau)+f(\tau)\,\mathrm{d}\tau \tag{11}$$

Equations (10) and (11) are combined to yield

$$\mathrm{d}J=\phi_x\delta x+(\phi_x f-L)\,|_{\tau}\mathrm{d}\tau+\int_{\tau}^{0}(L_x\delta x+L_u\delta u+L_p\delta p)\,\mathrm{d}t \tag{12}$$

It is necessary to find a relation between δx and $\mathrm{d}\tau$ to eliminate the $\mathrm{d}\tau$ term in Eq. (12). Solution of the optimization problem requires integration of the state x from time = 0 until time = τ. Termination of the state integration is determined by some cutoff condition at $t=\tau$, since τ is a free quantity not known a priori. Suppose $\Omega(x(\tau))$ is such a cutoff condition. Let

$$\Omega(x(\tau))=0 \tag{13}$$

Perturbation, expansion, simplification, use of Eq. (11), and solution for $\mathrm{d}\tau$ yields

$$\mathrm{d}\tau=-\Omega_x\delta x(\tau)/\Omega_x f \tag{14}$$

Substitution of Eq. (14) into Eq. (12) yields

$$\mathrm{d}J=\left(\phi_x-\frac{(\phi_x f-L)}{\Omega_x f}\Omega_x\right)|_{\tau}\delta x(\tau)+\int_{\tau}^{0}(L_x\delta x+L_u\delta u+L_p\delta p)\,\mathrm{d}t \tag{15}$$

The adjoint equation, with variable substitution for simplification, is

$$\dot{\lambda}=\frac{\mathrm{d}\lambda}{\mathrm{d}t}=-F^T\lambda-L_x^T \tag{16}$$

and one has

$$\frac{\mathrm{d}}{\mathrm{d}t}(\lambda^T\delta x)=\dot{\lambda}^T\delta x+\lambda^T\delta\dot{x} \tag{17}$$

Use of Eq. (17) requires that a representation of $\delta\dot{x}$ be developed, but $\dot{x}$ can change discontinuously due to the switch points at t_s. This can be treated by considering the influence on $\dot{x}$ of each of the switch points separately.

Define

$$\delta x=\delta x_0+\sum_i\delta x_i \tag{18}$$

where x_0 is the state value without switch point contributions, and x_i is the state contribution due to switch point i. Making further variable substitutions and recognizing $\delta u=\delta p=0$ for the variation of x_i, one can show that

$$\delta\dot{x}_0=F\delta x_0+G\delta u+K\delta p \qquad \delta\dot{x}_i=F\delta x_i \tag{19}$$

Substitution of Eqs. (19) and (16) into Eq. (17), and simplification and use of Eq. (18) gives

$$\frac{\mathrm{d}}{\mathrm{d}t}(\lambda^T\delta x)=-L_x\delta x+\lambda^T(G\delta u+K\delta p) \tag{20}$$

Since the desired state at $t=0$ is specified explicitly, Eq. (18) yields

$$\delta x(0)=\delta x_0(0)=\delta x_i(0)=0 \tag{21}$$

Integration of Eq. (17) from $t=\tau$ to $t=0$ can now be done using Eq. (21), and recognizing the effects of integration across discontinuities at t_s. The integration yields

$$-\lambda^T(\tau)\delta x_0(\tau)-\sum_i\lambda^T(t_{s_i})\,\delta x_i(t_{s_i})=\int_{\tau}^{0}(-L_x\delta x+\lambda^T(G\delta u+K\delta p))\,\mathrm{d}t \tag{22}$$

By geometric argument, it can be shown that

$$\delta x_i(t_{s_i})=-(f_{s_i}^{+}-f_{s_i}^{-})\,\mathrm{d}t_{s_i} \tag{23}$$

Since the switch points have no effect at $t=\tau$, one has

$$\delta x_0(\tau)=\delta x(\tau) \tag{24}$$

Substituting Eqs. (24) and (23) into Eq. (22) and comparing the result and Eq. (15) implies that an appropriate definition for $\lambda(\tau)$ is

$$\lambda^T(\tau)=-\left(\phi_x-\frac{\phi_x f-L}{\Omega_x f}\Omega_x\right)\Big|_{\tau} \tag{25}$$

Equations (9) and (25) are applied to simplify the integrated equation, and the time-invariant property of p is used to yield

$$\mathrm{d}J=\int_{\tau}^{0}H_u\delta u\,\mathrm{d}t+\left(\int_{\tau}^{0}H_p\,\mathrm{d}t\right)\delta p-\sum_i\lambda^T(t_{s_i})\,(f_{s_i}^{+}-f_{s_i}^{-})\,\mathrm{d}t_{s_i} \tag{26}$$

Up to this point the problem has assumed a specified state at $t=0$ and a free state at terminal time. Typically, however, the terminal time state is constrained in some manner that may include a dependence on the parameter vector p. This is treated by creating a set of functions that establish a gradient contribution in the desired control, parameter, and transition time variations as a function of the violations of the constraints.

The equality constraint vector [exclusive of Ω in Eq. (13)] is

$$\Psi=\Psi(x(\tau),p(\tau))=\Psi(x(\tau),p)=0 \tag{27}$$

Differentiating Eq. (27), use of Eq. (11), and the time invariance of p yields

$$\mathrm{d}\Psi=\Psi_x(\delta x(\tau)+f(\tau)\,\mathrm{d}\tau)+\Psi_p\delta p \tag{28}$$

A matrix set of differential equations that will incorporate the results of Eq. (28) and propagate the influence of the equality constraints through the vehicle trajectory and geometry satisfies the adjoint differential equation

$$\dot{\Lambda} = -A^T \Lambda \tag{29}$$

with the definition of A selected to separate state and parameter equality constraint sensitivity effects.

$$A = \begin{bmatrix} f_x & f_p \\ 0 & 0 \end{bmatrix} \tag{30}$$

Equations (30), (29), and (19) can be used to show

$$\frac{\mathrm{d}}{\mathrm{d}t}\left(\Lambda^T \begin{pmatrix} \delta x \\ \delta p \end{pmatrix}\right) = \Lambda^T \begin{pmatrix} G\delta u \\ 0 \end{pmatrix} \tag{31}$$

Integration of Eq. (31), use of Eq. (21), and substitution of Eq. (23) into the result yields

$$\Lambda^T(0)\begin{pmatrix} 0 \\ \delta p \end{pmatrix} - \Lambda^T(\tau)\begin{pmatrix} \delta x(\tau) \\ \delta p \end{pmatrix} = \int_\tau^0 \Lambda^T \begin{pmatrix} G\delta u \\ 0 \end{pmatrix} \mathrm{d}t - \sum_i \Lambda^T(t_{s_i}) \begin{bmatrix} (f_{s_i}^+ - f_{s_i}^-)\,\mathrm{d}t_{s_i} \\ 0 \end{bmatrix} \tag{32}$$

For convenience, Λ is partitioned into two separate matrices

$$\Lambda = \begin{bmatrix} \Lambda_1 \\ \Lambda_2 \end{bmatrix} \tag{33}$$

Substitution of Eq. (33) into Eq. (32) yields

$$-\Lambda_1^T(\tau)\delta x(\tau) + (\Lambda_2^T(0) - \Lambda_2^T(\tau))\delta p = \int_\tau^0 \Lambda_1^T G\delta u \mathrm{d}t - \sum_i \Lambda_1^T(t_{s_i})\,(f_{s_i}^+ - f_{s_i}^-)\,\mathrm{d}t_{s_i} \tag{34}$$

Substitution of Eq. (14) into Eq. (28) yields

$$\mathrm{d}\Psi = \left(\Psi_x - \frac{\Psi_x f \Omega_x}{\Omega_x f}\right)\delta x + \Psi_p \delta p \tag{35}$$

Comparing the forms of Eq. (34) with Eq. (35), it is clear that useful definitions of the boundary conditions are

$$\Lambda_1^T(\tau) = -(\Psi_x - \Psi_x f \Omega_x / \Omega_x f) \qquad \Lambda_2^T(\tau) = -\Psi_p \tag{36}$$

Substitution of Eqs. (36) into Eq. (34) and, subsequently, the result into Eq. (35) yields

$$\mathrm{d}\Psi = \int_\tau^0 \Lambda_1^T G\delta u \mathrm{d}t - \Lambda_2^T(0)\delta p - \sum_i \Lambda_1^T(t_{s_i})\,(f_{s_i}^+ - f_{s_i}^-)\,\mathrm{d}t_{s_i} \tag{37}$$

A certain amount of notational simplicity is useful for future manipulation. The following definitions are therefore useful:

$$g = \begin{bmatrix} \int_\tau^0 H_p^T \mathrm{d}t \\ -\lambda^T(t_{s_1})\,(f_{s_1}^+ - f_{s_1}^-) \\ -\lambda^T(t_{s_2})\,(f_{s_2}^+ - f_{s_2}^-) \\ \vdots \end{bmatrix} \qquad \delta v = \begin{bmatrix} \delta p \\ \mathrm{d}t_{s_1} \\ \mathrm{d}t_{s_2} \\ \vdots \end{bmatrix}$$

$$M = [-\Lambda_2^T(0) \mid -\Lambda_1^T(t_{s_1})(f_{s_1}^+ - f_{s_1}^-) \mid -\Lambda_1^T(t_{s_2})(f_{s_2}^+ - f_{s_2}^-) \mid \cdots] \tag{38}$$

Substitution of Eqs. (38) into Eqs. (37) and (26) yields

$$\mathrm{d}J = \int_\tau^0 H_u \delta u \mathrm{d}t + g^T \delta v \qquad \mathrm{d}\Psi = \int_\tau^0 \Lambda_1^T G\delta u \mathrm{d}t + M\delta v \tag{39}$$

Inspection of Eqs. (39) reveals that the desired decreases in J and $|\Psi|$ functionally imply desired variations in δu and δv. It is necessary to control the size of the steps taken by u and v, however, to assure that the first-order approximations made thus far do not prevent convergence to the extremal solution being sought.

An appropriate way to define step size is to create a quantity that is quadratic in δu and δv to assure a step whose measure is positive. Define

$$S^2 = \frac{1}{2}\int_\tau^0 \delta u^T U^{-1} \delta u \mathrm{d}t + \frac{1}{2}\delta v^T V^{-1} \delta v \tag{40}$$

It is appropriate to seek improvement in the equality constraint violations in direct proportion to the violations. Define

$$\mathrm{d}\Psi = -C_\Psi \Psi \tag{41}$$

The step size control, the constraint violation improvement, and the cost improvement relations must be unified into a single set of relations. This is accomplished by adjoining a combination of Eqs. (41), (40), and (39) with Lagrange multipliers.

At the extemal, the variation of the adjoined equation with respect to δu and δv vanishes. Since the separate variations are independent, they must separately vanish.

The following definitions are introduced:

$$I_{\Psi\Psi} = \int_\tau^0 \Lambda_1^T G U G^T \Lambda_1 \mathrm{d}t \qquad I_{\Psi J} = \int_\tau^0 \Lambda_1^T G U H_u^T \mathrm{d}t$$

$$I_{JJ} = \int_\tau^0 H_u U H_u^T \mathrm{d}t \tag{42a}$$

$$B = (I_{\Psi\Psi} + MVM^T)^{-1} \qquad C = (I_{\Psi J} + MVg) \tag{42b}$$

Manipulation of the adjoined equation, substitution of Eq. (42), and introduction of an adjoint function variable C_J yields

$$\delta u = U(-C_\Psi G^T \Lambda_1 B\Psi - C_J(H_u^T - G^T \Lambda_1 BC)) \tag{43a}$$

$$\delta v = -C_\Psi VM^T B\Psi - C_J(Vg - VM^T BC) \tag{43b}$$

An equation defining the value of C_J is necessary. It is appropriate to mathematically tie the value of C_J to the gradient equations and some suitable cost variation (a measure of step size). One therefore defines a specified cost variation $\mathrm{d}J_s$.

Using Eq. (43) and the first of Eqs. (39), substituting $\mathrm{d}J_s$ for $\mathrm{d}J$, reordering terms with substitution of Eq. (42) into the result, and solving for C_J, one gets

$$C_J = -\frac{\mathrm{d}J_s + C_\Psi(I_{\Psi J}^T B\Psi + g^T VM^T B\Psi)}{I_{JJ} - I_{\Psi J}^T BC + g^T Vg - g^T VM^T BC} \tag{44}$$

With $\mathrm{d}J_s$ somehow specified, use of Eqs. (44) and (43) permits one to evaluate δu and δv provided C_Ψ is computable. C_Ψ, however, is simply a value used to establish a rate at which the Ψ-vector violations are reduced.

Computer Results

A software implementation of the algorithm with dynamics and boundary conditions specified was developed and used to evaluate the characteristics of the optimal air-breathing vehicle as a function of different bounds on the inequality constraints.

Sample cases were run fixing the specific force bound while varying the dynamic pressure bound. Cases were also run fixing the dynamic pressure bound while varying the specific force bound. All cases imposed the same orbit and ground boundary conditions. The ground conditions chosen represent horizontal sea-level takeoff at an airspeed of 250 mph, chosen as a compromise between low takeoff speed to keep runway requirements down, and a lift requirement from the vehicle first stage to achieve flight with minimum wing size.

All cases assumed an eastward equatorial launch to equatorial orbit. A consequence of this assumption is also minimal energy required to achieve orbit.

Specific inequality constraints used in each case are provided in Table 1. Dynamic pressure bounds were chosen to cover the range of values considered reasonable for air-breathing vehicles in a wide range of studies. Specific force bounds were chosen to keep g loads endurable on passengers (the Space Shuttle limits are close to 600 psf and 3 g's).

The data from the optimization runs is presented tabularly and in plots. Tables 2-4 present the parameters, propulsive mode switch point times, relevant states at the transition points, and fuel consumption data for the cases run. Figures 1-7 present some interesting time and Mach number dependent variables.

A wide variety of physical effects influencing the optimization results are apparent upon inspection of the different cases run. These include effects resulting from aerodynamic properties of the first stage, and effects resulting from the influence of the inequality constraints.

The most striking similarity in all cases run is seen in Table 4. The fuel consumption is only weakly associated with the inequality constraint bounds used. In fact, given the slow terminal convergence of gradient algorithms, the difference in the propellant consumption numbers can be attributed as much to small differences in the degree of optimality achieved at the cutoff of the optimization algorithm as it can be associated with genuine physical effects. Therefore, within the range of inequality constraint bounds studied, fuel consumption effects of constraint-bound variations can be offset by vehicle configuration and trajectory changes.

Table 2 shows definite dynamic pressure related trends in many of the parameters. The fuselage width, the turbojet inlet, and the scramjet inlet all establish capture area for the air-breathing propulsion systems, and all grow with a decline in dynamic pressure bound. Comparison of altitudes as a function of Mach number for first-stage flight in Fig. 1 shows a steady altitude increase with the decrease in dynamic pressure bound until just before staging. These effects taken together permit the vehicle to hold down the dynamic pressure due to the lower air density at higher altitude while keeping reasonable levels of air-breathing thrust as a result of larger propulsion system intake. Table 4 shows fuel consumption to be relatively constant during air-breathing flight for all cases run. An increase in fuselage width, combined with the constraint to match ground propellant volume and tank volume, requires a decline in other fuselage dimensions. Thus, nose angle and fuselage length decrease. A secondary effect of increasing air-breathing propulsion system inlet size is to increase available thrust at takeoff, permitting somewhat

Table 1 Inequality constraints on computer runs

Case	Dynamic pressure bound, lbf/ft^2	Specific force bound, g's
I	1000	3.0
II	800	3.0
III	600	3.0
IV	800	2.5

Table 2 Parameter values

Physical parameter	Case I	Case II	Case III	Case IV
Nose angle, rad	0.01925	0.01909	0.01879	0.01912
Fuselage width, ft	34.3	35.2	35.7	34.9
Fuselage length, ft	151.6	150.9	149.5	151.0
TJ/SCRJ tank volume ratio	0.417	0.417	0.418	0.417
Turbojet inlet height, ft	9.66	10.25	10.74	9.92
Scramjet inlet height, ft	14.56	15.80	16.66	15.53
Wing span, ft	323	293	271	308
Delta wing angle, rad	1.340	1.272	1.344	1.313
Rocket fuel capacity, slugs	3.16×10^4	3.16×10^4	3.15×10^4	3.15×10^4
Maximum rocket thrust, lbf	1.724×10^6	1.738×10^6	1.820×10^6	1.726×10^6

Table 3 Propulsive mode switch point state functions

Case	Transition point, t_{si}	Altitude, ft$\times10^4$	Radial velocity, ft/s	Angular velocity, rad$\times10^{-4}$	Tangential airspeed, ft/s$\times10^3$
I	1	2.77	781	1.291	1.175
II	1	3.49	634	1.356	1.313
III	1	3.94	573	1.347	1.293
IV	1	3.24	702	1.301	1.196
I	2	7.82	136	2.31	3.32
II	2	7.55	103	2.32	3.33
III	2	7.48	43.1	2.30	3.30
IV	2	7.01	2.92	2.35	3.39
I	3	7.99	186	2.30	3.29
II	3	7.72	231	2.31	3.32
III	3	7.72	306	2.30	3.30
IV	3	7.18	344	2.33	3.36

Table 4 Ground value of propellant masses

Case	Turbojet fuel, slugs $\times 10^3$	Scramjet fuel, slugs $\times 10^2$	Rocket fuel, slugs $\times 10^4$
I	3.16	4.42	3.16
II	3.20	4.45	3.16
III	3.14	4.36	3.15
IV	3.17	4.43	3.15

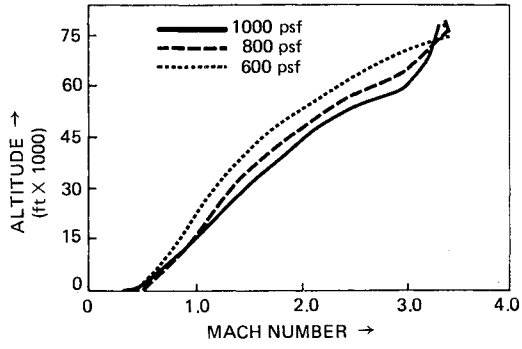

Fig. 1 Altitude vs Mach number through first-stage flight: specific force bound = 3 g's, dynamic pressure bound varied.

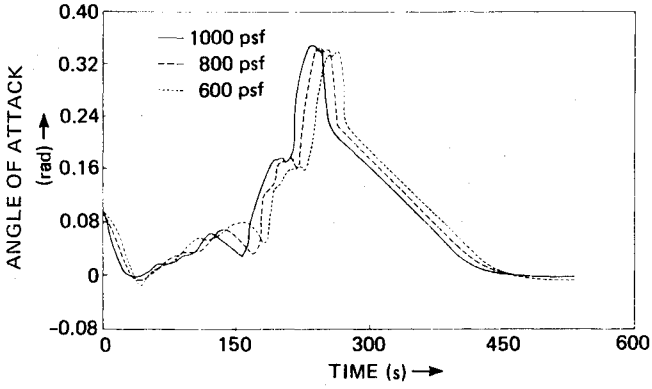

Fig. 2 Angle of attack vs t for full flight time: specific force bound = 3 g's, dynamic pressure bound varied.

reduced wing lift capability for the vehicle. A decline in the wing span results with reduced dynamic pressure bound reflecting the lower lift requirements when combined with the delta wing sweep angle and the lift coefficient.

Table 3 shows that the general altitude range at the transition points is similar in all cases, with the altitude changing little between turbojet shutdown and staging (t_{s_2} and t_{s_3}, respectively).

Referring to Table 4, it is apparent that the high specific impulse of the air-breathing system when compared to the rocket leads to the vast bulk of the propellant consumption occurring during rocket flight in spite of the substantial velocity contributions of the first stage. This implies that the air-breathing propulsion is very desirable, since a large gain in system energy is achieved with a relatively small fuel expenditure. It also suggests that significant air-breathing system improvements will only marginally improve overall system fuel usage.

Inspection of Fig. 2 (cases I-III) shows consistent early angle-of-attack patterns during air-breathing flight. All cases start with relatively high angle of attack to achieve necessary lift for takeoff. The angle of attack subsequently undergoes a continuous decline in the first 35-45 s to a slightly negative value. The nadir of the angle-of-attack plots consistently occur in the transonic region (between $M = 1.0$ and $M = 1.2$)

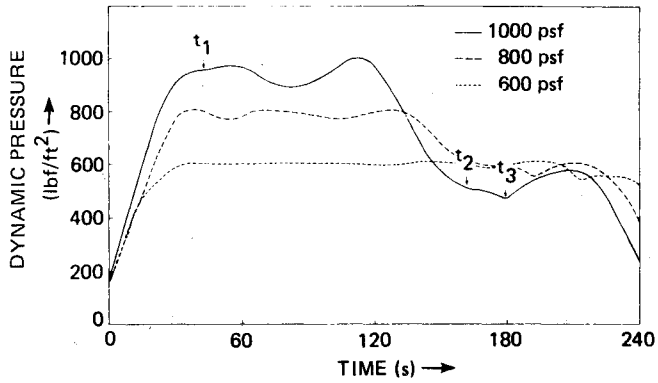

Fig. 3 Dynamic pressure vs t through dense atmosphere: specific force bound = 3 g's, dynamic pressure bound varied.

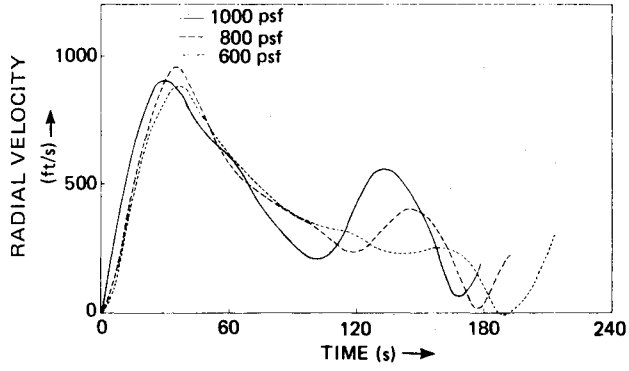

Fig. 4 Radial velocity vs t through first-stage flight: specific force bound = 3 g's, dynamic pressure bound varied.

where the drag coefficient peaks. This is the consequence of the utilization of stored potential energy (altitude) combined with thrust to rapidly go through the most dissipative aerodynamic flight region. An angle-of-attack increase follows to achieve climb, it peaks, then declines again as air-breathing thrust capability diminishes with altitude. The angle-of-attack bottoms out again at about the time when the turbojet shuts down. A pullup maneuver is then executed under scramjet power alone. The pullup orients the vehicle for effective use of the rocket power at staging. Since the rocket uses fuel much more rapidly than the air-breathing engines, improper rocket orientation can lead to inefficient use of rocket fuel to achieve a substantial change in flight-path angle. There is a consistent large peak in the early phase of rocket flight followed by a dropoff to near zero. This effect is a consequence of the need to achieve a substantial radial velocity component in order to obtain the desired altitude at rocket burnout. The dropoff in angle-of-attack near the flight end is a consequence of an increasing use of gravity turning prior to orbit insertion. It is interesting, however, to note the differences in the pairs of air-breathing flight angle-of-attack valleys, the magnitudes of which are secondary effects of wing lift capability. In the transonic negative angle-of-attack region a more negative angle-of-attack is permitted for tighter dynamic pressure bounds. The result is similar net negative lift, and similar first peak radial velocity behavior, seen in Fig. 4, plotting the same three cases, eventually leading to similar terminal first-stage states. The second angle-of-attack valley is just prior to prerocket ignition pullup. Reduced wing lift capability results in a somewhat greater angle-of-attack to help keep up the net lift for the flight phase immediately preceding the aerodynamic pullup maneuver. In spite of the higher angle-of-attack, net lift does decline with wing span in the flight region before the second radial velocity peak. The reduced lift also pulls down the magnitude of the second peak and causes lower radial velocities just before the aerodynamic pullup.

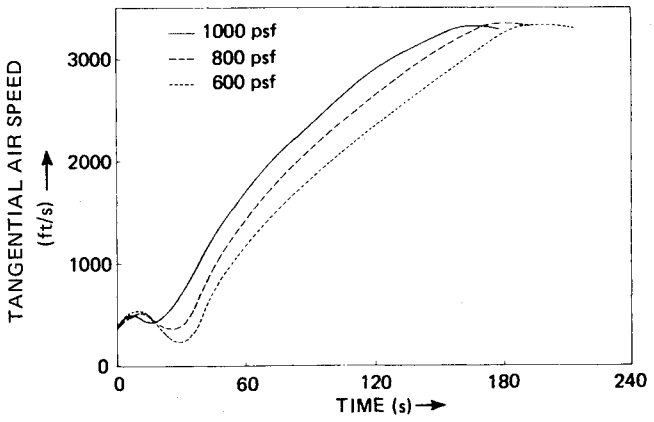

Fig. 5 Tangential airspeed vs t through first-stage flight: specific force bound 3 g's, dynamic pressure bound varied.

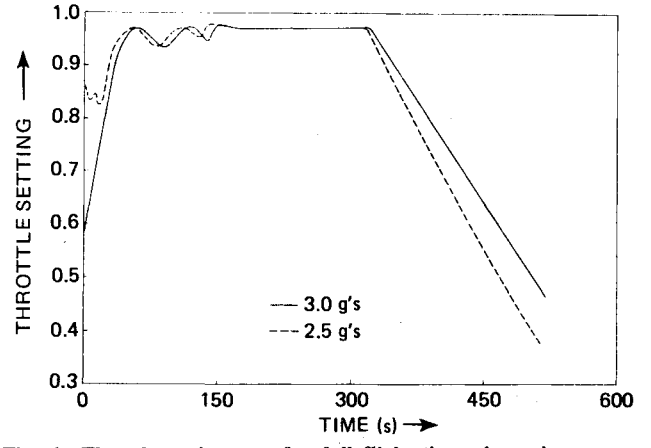

Fig. 6 Throttle setting vs t for full flight time: dynamic pressure bound = 800 psf, specific force bound varied.

Staging consistently occurs between $M=3.3$ and $M=3.5$. At these low Mach numbers the scramjet has low mass capture and therefore low power. Consistency of the staging Mach number is itself an extremely important effect. Its value suggests that the scramjet provides little net benefit while contributing a high dry mass penalty to the first stage. Recalling that the scramjet mass model is based on the high mass of a system capable of tolerating the thermal load of high Mach numbers, this conclusion may in part be a consequence of design conservatism.

The time-dependent variable plots show a great deal of dynamic pressure bound related structure. Figure 3, plotting cases I-III, shows the dynamic pressure plotted through dense atmospheric flight. The most obvious effect is the close tracking of the dynamic pressure bounds, in all cases, until the decline in atmospheric density reduces the value below the bound for the remainder of flight. With less stringent constraints the bound is less precisely tracked. This is a result of the vehicle's ability to more closely approximate the desired unconstrained behavior. As the bound is decreased, more time is spent near the limit, which is a consequence of greater constraints on acceleration. In addition, the dynamic pressure plots all show a temporary rise in dynamic pressure after staging as a result of velocity increase effects initially exceeding the atmospheric density decreases with altitude when the vehicle begins the high rate of rocket acceleration.

In Fig. 4 (covering only first-stage flight), a persistent double-peak effect and prestaging climbout is seen. The first peak is a consequence of the transonic negative angle-of-attack followed by a need to stay in a sufficiently dense atmosphere to hold turbojet thrust levels high, permitting continued tangential velocity acceleration. The second peak is

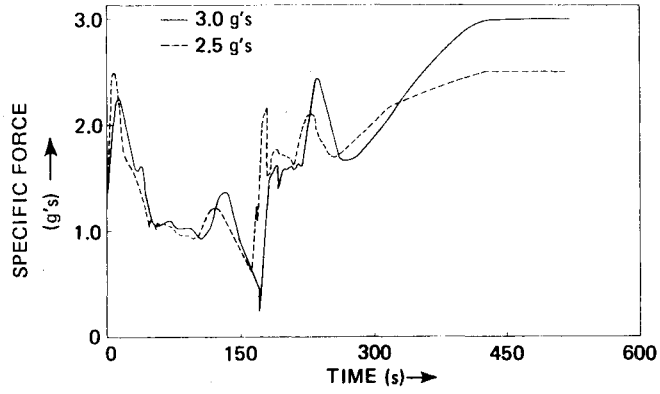

Fig. 7 Specific force vs t for full flight time: dynamic pressure bound = 800 psf, specific force bound varied.

a consequence of Mach number associated gains in the rate of mass capture, which permits higher altitude flight with continued acceleration. The pullup, as discussed earlier, permits optimal vehicle orientation for rocket ignition.

Figure 5, the tangential airspeed through first-stage flight (also showing cases I-III) shows consistent acceleration except early and late in flight. The acceleration demonstrates that the main orbital energy benefit from the first stage comes in the tangential velocity component. The late velocity dropoff is a consequence of a combination of atmospheric rarefaction, reducing thrust, and, finally, an aerodynamic energy transfer to radial velocity to achieve vehicle pullup. The early flight tangential velocity dip is associated with dynamic pressure vehicle load relief. The vehicle with a reduced dynamic pressure bound needs to achieve higher altitude early in flight to keep air density down, as seen in Fig. 1, controlling the dynamic pressure magnitude. The radial velocity component is given preference to achieve an altitude increase. Therefore, as the bound is reduced, greater emphasis is put on the radial component, leading to less energy being fed into the tangential component. The result, when aerodynamic dissipation is included, is a greater dip in magnitude of the tangential airspeed.

Figure 6 is the fuel throttle settings for cases II and IV. It shows a characteristic throttled-down setting at takeoff to prevent excessive vehicle loading that could result from the high mass capture rate and high lift that the dense atmosphere and high angle-of-attack induce. The throttle setting increases subsequently to achieve high thrust through the dissipative transonic region, followed by a slight throttling down in the less dissipative supersonic environment, and then a move toward maximum thrust is made (hence maximum acceleration) until specific force effects dominate in the late phases of rocket flight. The failure to achieve full throttle settings (max = 0.97 rather than 1.00) is a consequence of the slow terminal convergence of the gradient algorithm to the optimum and the optimization algorithm cutoff point. The cause of the continuous decline in throttle setting in the later phase of rocket flight is clearly seen in Fig. 7, which plots the same cases. It is the need to stay within the specific force bound as the rocket mass declines. Figure 6 shows that the lower specific force bound results in a steeper decline in throttle setting, a consequence of similar rocket stage mass properties and maximum rocket thrust magnitudes, with substantially reduced acceleration bounds.

Comments about the Scramjet

The low staging Mach number in all cases run on the computer provides little support for use of a scramjet in a vehicle with the flight profile and configuration studied. However, this should not be interpreted as a universal condemnation of the supersonic combustion propulsion system.

The turbojet system model includes a rapid dropoff of specific impulse near the staging Mach number. When this

effect is coupled with the dynamic pressure constraint, thrust diminishes rapidly. The scramjet mass capture ratio remains well below unity, limiting its thrust contribution, and forcing vehicle staging to sustain acceleration under rocket power.

Several changes in the vehicle design considerations could change the scramjet contributions. These include: 1) use of a rocket in the first stage, or a single-stage-to-orbit vehicle, which could overlap with air-breathing propulsion; 2) development of a higher temperature-tolerant turbojet system, with the resulting higher impulse; 3) reduction in scramjet system mass by development of lightweight high-temperature-tolerant materials (i.e., ceramics).

Conclusions

It has been demonstrated that a gradient-type algorithm incorporating several classes of controls, including time-varying control histories, time-invariant design parameters, and locations of dynamic discontinuities, and permitting application of equality and inequality constraints can be successfully applied to a design problem involving complex system dynamics.

The algorithm has been successfully implemented on a digital computer and applied to a hypothetical two-stage launch vehicle with an air-breathing first stage and a rocket second stage.

Fuel consumption of the proposed launch vehicle is relatively insensitive to substantial variations in the inequality constraint bounds on dynamic pressure and specific force when vehicle geometry modifications, propulsion mode change time modifications, and trajectory changes are all allowed to accommodate the constraint-bound variations.

In all cases examined, the staging Mach number (i.e., transition from air-breathing flight to rocket flight) occurred between $M=3.3$ and $M=3.5$. This relatively low staging Mach number, in spite of the availability of a supersonic combustion ramjet, implies that little is gained from an air-breathing system suited to high Mach number flight. Turbojet power alone in the first stage, followed by rocket flight, is likely to provide similar performance with a less complex system. These effects may, however, be propulsion system mass model dependent.

Highly variable throttle settings in the propulsion systems are necessary to accommodate the specific force bounds imposed on the vehicle. The effect is particularly obvious in the later stages of rocket flight when the bound is followed in spite of declining system mass.

Reducing the dynamic pressure bound expands the air-breathing propulsion system inlets and raises the early low Mach number flight altitude, though staging states are very similar. Air-breathing propulsion fuel consumption is small for the substantial velocity gain that results.

There is no reason to suppose that application of other inequality constraints will produce results any less interesting. The general approach seems to work well with definite trends apparent after a limited number of optimization cases are run to completion.

Acknowledgments

This paper was prepared under Contract NAS9-13809 with the National Aeronautics and Space Administration. Publication of this paper does not constitute approval by NASA of the findings or conclusions contained herein.

References

[1] Hankey, W.L., "Some Design Aspects of Hypersonic Vehicles," Aerospace Research Laboratories Rept. No. 70-0049, March 1970.

[2] Bryson, A.E. and Ross, S.E., "Optimum Rocket Trajectories with Aerodynamic Drag," *Jet Propulsion,* Vol. 28, July 1958, pp. 465-469.

[3] Bryson, A.E. and Denham, W.F., "A Steepest-Ascent Method for Solving Optimum Programming Problems," *Journal of Applied Mechanics,* June 1962, pp. 247-257.

[4] Wilhite, A.W., "Optimization of Rocket Propulsion Systems for Advanced Earth-to-Orbit Shuttles," *Journal of Spacecraft and Rockets,* Vol. 17, No. 2, March-April 1980, pp. 99-104.

[5] Hattis, P.D., "An Optimal Design Methodology for a Class of Air-Breathing Launch Vehicles," Ph.D. Thesis, Massachusetts Institute of Technology, June 1980.

[6] Martin, J.A., "Aerospaceplane Optimization and Performance Estimation," Master's Thesis, Massachusetts Institute of Technology, Aug. 1967, p. 9.

[7] Jones, R.A. and Huber P.W., "Toward Scramjet Aircraft," *Astronautics & Aeronautics,* Vol. 16, Feb. 1978, p. 46.

[8] Jones, R.A. and Huber, P.W., "Airframe Integrated Propulsion System for Hypersonic Cruise Vehicles," paper A79-20076, presented at 11th Congress of the International Council of the Aeronautical Sciences, Vol. 1, Sept. 1978, pp. 130-136.

[9] Nicolai, L.M., *Fundamntals of Aircraft Design,* E.P. Domicone Printing Services, Fairborn, Ohio, pp. E4-E5.